Bioconjugate Chemistry

Article

pubs.acs.org/bc

Synthesis and Characterization of Macromolecular Rhodamine Tethers and Their Interactions with P-Glycoprotein

Lindsey Crawford[†] and David Putnam*[,†,‡]

[†]School of Chemical and Biomolecular Engineering and [‡]Department of Biomedical Engineering, Cornell University, Ithaca, New York 14853, United States

Supporting Information

ABSTRACT: Rhodamine dyes are well-known P-glycoprotein (P-gp) substrates that have played an important role in the detection of inhibitors and other substrates of P-gp, as well as in the understanding of P-gp function. Macromolecular conjugates of rhodamines could prove useful as tethers for further probing of P-gp structure and function. Two macromolecular derivatives of rhodamine, methoxypolyethylene glycol-rhodamine6G and methoxypolyethylene glycol-rhodamine123, were synthesized through the 2′-position of rhodamine6G and rhodamine123, thoroughly characterized, and then evaluated by inhibition with verapamil for their ability to interact with P-gp and to act as efflux substrates. To put the results into context, the P-gp interactions of the new conjugates were compared to the commercially available methoxypolyethylene glycol-rhodamineB. FACS analysis confirmed that macromolecular tethers of rhodamine6G, rhodamine123, and rhodamineB were accumulated in P-gp expressing cells 5.2 ± 0.3%, 26.2 ± 4%, and 64.2 ± 6%, respectively, compared to a sensitive cell line that does not overexpress P-gp. Along with confocal imaging, the efflux analysis confirmed that the macromolecular rhodamine tethers remain P-gp substrates. These results open potential avenues for new ways to probe the function of P-gp both *in vitro* and *in vivo*.

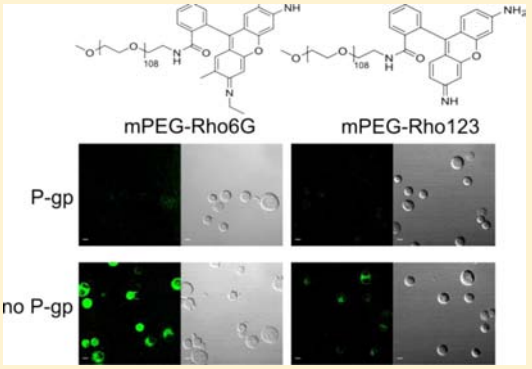

INTRODUCTION

P-glycoprotein (P-gp) is an ATP-binding cassette membrane efflux protein that actively transports small molecules across the cell membrane. It is expressed in both healthy (e.g., gastrointestinal endothelium) and diseased (e.g., multidrug resistant cancer) tissues.[1−3] Although general characteristics of P-gp substrates are known, such as high lipophilicity, the protein is fairly promiscuous and transports a surprisingly wide range of structures.[4,5] The clinical ramifications of P-gp expression in cancers are well documented and the literature is replete with examples of drug targeting with antibodies against P-gp expressing cell types[6,7] or of attempts to inhibit P-gp mediated efflux of substrates.[8] However, to date the clinical impacts of these approaches have yet to be fully realized. For these reasons, probes to evaluate the functionality of P-gp are increasingly important to help better understand the mechanism and specificity of its activity.[9,10] In particular, polymeric probes could prove useful for *in vivo* applications since the majority of probes are small molecules that often have limited circulation time.[11,12]

Polymeric materials have been extensively studied for their ability to inhibit P-gp.[13] Poloxamers are a particularly well-known class of polymeric P-gp inhibitors.[14] Poloxamers inhibit P-gp by either decreasing membrane fluidity or depleting ATP.[15] The polymers do not directly interact with P-gp and are not considered substrates of the protein. Little is known about polymers acting as substrates of P-gp, and our aim is to describe such interactions through the conjugation of polymers to established low molecular weight substrates of P-gp.

Rhodamine dyes are one popular class of P-gp substrates. The rhodamine variant, rhodamine123, is a strong P-gp substrate and is particularly well represented in the literature as a probe to quantify the activity of the protein under different conditions.[16−18] Rhodamine123 (Rho123) has played a historic role in the detection of P-gp inhibitors and in the analysis of potential treatments for multi-drug-resistant (MDR) cancers.[19−22] Although Rho123 is more widely used as a P-gp substrate, other rhodamine variants have been explored for affinity to P-gp. Rhodamine 6G (Rho6G) and Rhodamine B (RhoB) have also been used as P-gp substrates and have higher and lower affinity, respectively, to P-gp than Rho123.[16] An expansion of the potential use of rhodamines could lead to opportunities for further investigation into P-gp function. One useful expansion would be conjugation of a macromolecule to rhodamine variants. Early conjugates of rhodamine derivatives were synthesized by activation of the 4′ or 5′ sites,[23,24] but more recently a one-step substitution of small compounds through the 2′ position of Rho6G and Rho123 was reported.[25]

Herein we report the synthesis and characterization of a methoxypolyethylene glycol (mPEG) conjugate of Rho6G and

Received: May 15, 2014
Revised: July 17, 2014
Published: July 22, 2014

   dx.doi.org/10.1021/bc5002196 | *Bioconjugate Chem.* 2014, 25, 1462−1469

Rho123 through the 2′ position and characterize their interactions with P-gp (Figure 1a,b). PEG is a well-established

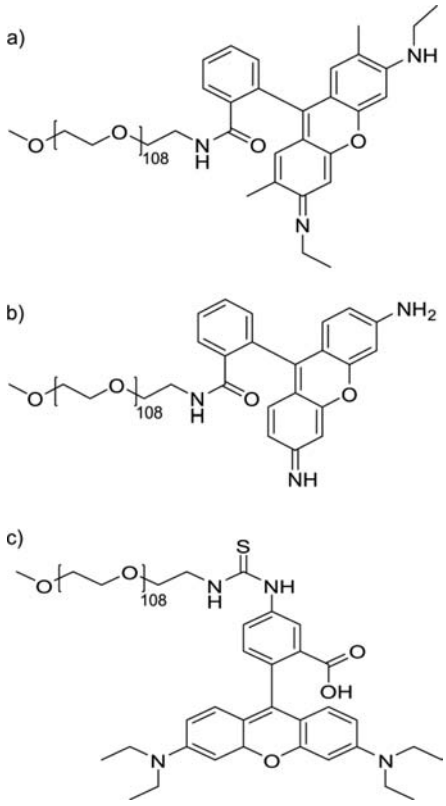

Figure 1. Proposed structure of (a) mPEG-Rho6G conjugate, (b) mPEG-Rho123 conjugate, and (c) commercially available mPEG-RhoB.

tether of small molecules, peptides, and proteins,[11,26] and mPEG-Rho6G and mPEG-Rho123 conjugates could be useful to investigators in the P-gp field. We also compare the P-gp interaction of the 2′-substituted mPEG-Rho6G and mPEG-Rho123 to the more common and commercially available 4′-substituted mPEG-RhoB (Figure 1c). Recognizing that perturbations of the molecular architecture of a P-gp substrate can influence the interaction with P-gp,[27] we sought to establish the retained activity of the macromolecular rhodamine conjugates using the P-gp expressing breast adenocarcinoma cell line, MDA-435/LCC6 MDR. Our results show that PEG was effectively linked to Rho6G and Rho123 in a single step as determined by both ^{1}H NMR and diffusion ordered NMR. Additionally, retention of the P-gp interaction with the mPEG-Rho6G, mPEG-Rho123, and mPEG-RhoB conjugates was confirmed by both FACS analysis and confocal microscopy. Both techniques showed that the P-gp interaction with the conjugates directly correlated to that of free Rho6G, Rho123, and RhoB, thereby establishing the potential use of these macromolecular tethers of rhodamine derivatives as P-gp interactive conjugates.

RESULTS

Synthesis and Characterization of mPEG-Rho123 and mPEG-Rho6G. The conjugates of mPEG-Rho6G and mPEG-Rho123 were characterized by ^{1}H NMR (Supporting Information (SI) Figure S1 and Figure S2 respectively) and diffusion ordered NMR (Figure 2 and Figure 3 respectively).

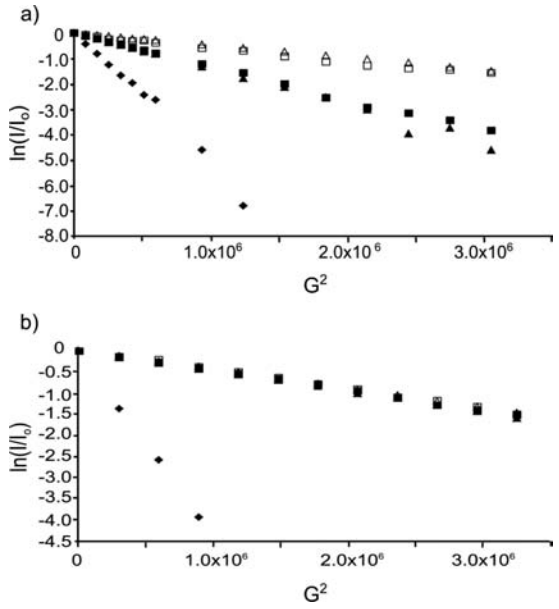

Figure 2. Stejskals-Tanner plots of diffusion ordered NMR. (■) Rho6G peak at 6.95 ppm, (▲) Rho6G peak 1.25 ppm, (□) mPEG peak at 3.17 ppm, (Δ) mPEG peak at 3.44 ppm, (♦) DMSO-d_6. (a) Free Rho6G and unconjugated mPEG-NH_2. Free Rho6G diffuses faster than mPEG-NH_2. (b) Conjugated mPEG-Rho6G. Covalent attachment is evident from the equal diffusion of Rho6G peaks and mPEG peaks.

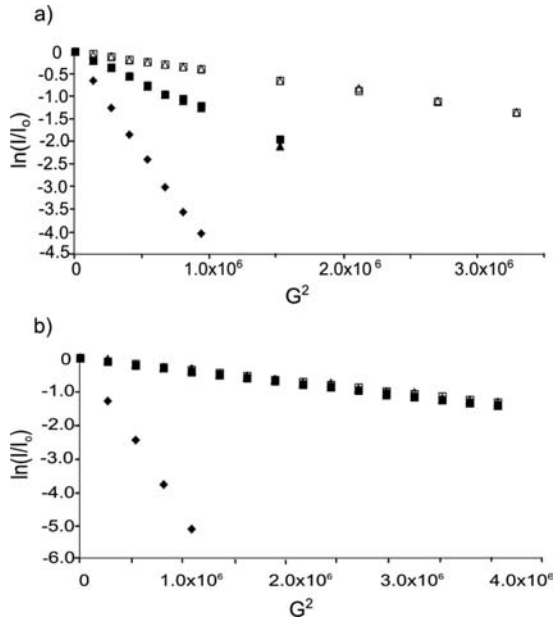

Figure 3. Stejskals-Tanner plots of diffusion ordered NMR. (■) Rho123 peaks at 6.14 and 6.16 ppm, (▲) Rho123 peaks at 6.09 and 6.10 ppm, (□) mPEG peak at 3.17 ppm, (Δ) mPEG peak at 3.44 ppm, (♦) DMSO-d_6. (a) Free Rho123 and unconjugated mPEG-NH_2. Free Rho123 diffuses faster than mPEG-NH_2. (b) Conjugated mPEG-Rho123. Covalent attachment is evident from the equal diffusion of Rho123 peaks and mPEG peaks.

The single proton NMRs (SI Figures S1 and S2) show the respective Rho6G and Rho123 peaks visible from a chemical shift between 5 and 8 ppm (aromatic region). Percent conjugation yields were ~90% (of polymer chains that were initially NH_2 terminated), calculated from peaks at 3.17 (from

dx.doi.org/10.1021/bc5002196 | Bioconjugate Chem. 2014, 25, 1462−1469

mPEG), 1.25 (from Rho6G), and 6.14 and 6.16 (from Rho123) ppm. To confirm that the ^{1}H NMR results were not from an unconjugated mixture of mPEG-NH_2 and free Rho6G or free Rho123 and that covalent conjugates were made, diffusion ordered NMR (which calculates relative diffusion of each peak in the spectra) was also performed (Figures 2 and 3). Small molecules, like free Rho6G or free Rho123, diffuse fast relative to macromolecules, like mPEG-NH_2. NMR signals with equal diffusion rates are indicative of covalently linked compounds. Diffusion ordered spectra of Rho6G with mPEG-NH_2 (Figure 2A), of conjugated mPEG-Rho6G (Figure 2B), of Rho123 with mPEG-NH_2 (Figure 3A), and of conjugated mPEG-Rho123 (Figure 3B) were obtained and represented by Stejskals-Tanner plots. The results show that Rho6G and Rho123 are covalently conjugated to the mPEG-NH_2 tether.

P-glycoprotein Interactions. The interaction between the mPEG-Rho6G, mPEG-Rho123, and mPEG-RhoB conjugates and P-gp was investigated using two MDA-435/LCC6 cell lines: MDA-435/LCC6 MDR which expresses P-gp and MDA-435/LCC6 WT which does not.[28] Before tests were initiated, P-gp expression in both MDR and WT cells was confirmed by Western blot (Figure 4). The Western blot confirms the expression of P-gp in the MDR cells and the lack of expression in WT cells. The protein band in the MDR cells is visible around the molecular weight of P-gp, 170 kDa, which correlates to the reported molecular weight of the protein.[29]

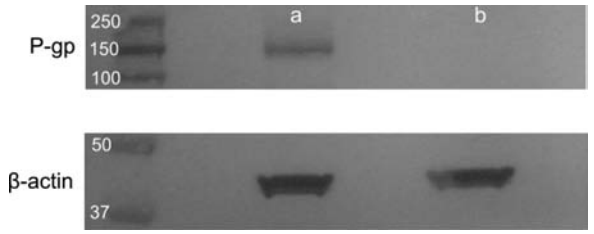

Figure 4. Western blot analysis to show P-gp expression in MDA-435/LCC6 MDR cells (a) and absence in MDA-435/LCC6 WT cells (b). A β-actin control was run for protein content comparison. The first lane is a protein ladder for reference with molecular weights in kDa.

Representative quantification of mPEG-Rho6G, mPEG-Rho123, and mPEG-RhoB accumulation in MDR and WT cells was obtained via FACS experiments and represented as a quantitated ratio between mean fluorescence of MDR cells compared to WT cells (Figure 5). Initial FACS experiments were conducted at 37 °C with 0 μM verapamil to investigate the efflux of both mPEG-dye conjugates and free dyes from MDR cells compared with WT cells. It was determined that 5.2 ± 0.3%, 26.2 ± 4%, and 64.2 ± 6% of mPEG-Rho6G, mPEG-Rho123, and mPEG-RhoB, respectively, accumulated in MDR cells in comparison to WT cells. Native dyes showed that 3.3 ± 0.4%, 9.7 ± 0.6%, and 59.2 ± 4% of Rho6G, Rho123, and RhoB, respectively, accumulated in MDR cells in comparison to WT cells. To show that the mechanism of efflux was mediated by P-gp, a series of verapamil (a well-established P-gp inhibitor[30]) concentrations (5, 25, 50, 75, and 100 μM) were added to the incubations. A concentration of 25 μM of verapamil increased MDR cell accumulation to 13.0 ± 1%, 59.8 ± 4%, and 93.6 ± 9% for mPEG-Rho6G, mPEG-Rho123, and mPEG-RhoB, respectively, and 28.5 ± 3%, 35.3 ± 2%, and 59.5 ± 9% for Rho6G, Rho123, and RhoB, respectively, compared to WT cells. FACS analysis was also performed with incubation at 4 °C to investigate endocytosis as the mechanism of cellular entry for mPEG-dye conjugates (Figure 6). Internalization of Rho6G, Rho123, and RhoB was decreased by 1.2 ± 0.06, 3.8 ± 0.3, and 1.2 ± 0.09 times in WT cells. Note that the y-axis for the RhoB experiment (Figure 6e) is smaller than the others in Figure 6. While these data appear to show that RhoB has lower overall cellular accumulation, the lower y-axis values of Figure 6e are due to the lower quantum efficiency of RhoB compared to Rho6G and Rho123.[31] Internalization of mPEG-Rho6G, mPEG-Rho123, and mPEG-RhoB was decreased by 2.9 ± 0.2, 6.4 ± 0.09, and 2.7 ± 0.3 times in WT cells. The greater decrease in mPEG-rhodamine conjugates signals endocytosis as an internalization mechanism. Statistics represent the significant differences in MDR/WT accumulation ratio at a p-value of <0.01.

Visual verification of the FACS results was obtained by confocal microscopy of cells incubated with both mPEG-dye conjugates and free dyes (Figure 7). Images were taken of mPEG-dye conjugates and free dyes incubated with MDR and WT cells at 37 °C with 0 μM of verapamil P-gp inhibitor. Images were also obtained from identical incubations conducted in the presence of 25 μM of verapamil to observe the increase in accumulation of mPEG-dye conjugates and free dyes. All images visually verify the FACS results.

DISCUSSION

Rhodamine dyes are a class of well characterized P-gp substrates and have been utilized for numerous P-gp analysis studies. This study investigated the synthesis and P-gp mediated efflux patterns of macromolecular conjugates composed of mPEG linked through the 2′-position of Rho6G and Rho123 in comparison to the patterns of free Rho6G and free Rho123. This study also compared P-gp mediated efflux patterns of commercially available mPEG-RhoB in comparison to patterns of free RhoB. Conjugate synthesis was confirmed by ^{1}H NMR and diffusion ordered ^{1}H NMR. Both the mPEG and Rho6G or Rho123 peaks are present and identifiable on the ^{1}H spectra and the diffusion ordered NMR confirmed covalent conjugation. When free Rho6G or Rho123 is physically mixed with unconjugated mPEG-NH_2, the decrease in peak intensity in the diffusion ordered NMR is much faster for Rho6G or Rho123 peaks than for mPEG-NH_2 peaks, which translates into different diffusion rates and depicts a lack of covalent attachment. However, once Rho6G or Rho123 is conjugated to the mPEG, the decrease in intensity is the same for both the Rho6G or Rho123 and mPEG peaks, which depicts covalent attachment of the compounds. The behavior of faster decay for smaller molecules seen on the Stejskals-Tanner plots is a consistent result given the size of the molecules involved; the smaller the molecule, the faster the signal decays with increasing gradient.[32−34]

FACS experiments were performed to analyze efflux patterns of mPEG-Rho6G, mPEG-Rho123, and mPEG-RhoB and compare them with patterns of Rho6G, Rho123, and RhoB. The two wash steps allowed for measurements of efflux separate from any variances in influx. Results with 0 μM verapamil exhibit the pattern of Rho6G, Rho123, and RhoB acting as "high", "medium", and "low" P-gp substrates, respectively, corresponding to efflux patterns. This same pattern is followed by the mPEG conjugates where mPEG-RhoB has the highest accumulation in MDR cells compared to WT cells, mPEG-Rho123 has moderate accumulation, and mPEG-Rho6G has low accumulation. Studies in the literature involving Rho6G, Rho123, and RhoB report the same trend

dx.doi.org/10.1021/bc5002196 | Bioconjugate Chem. 2014, 25, 1462−1469

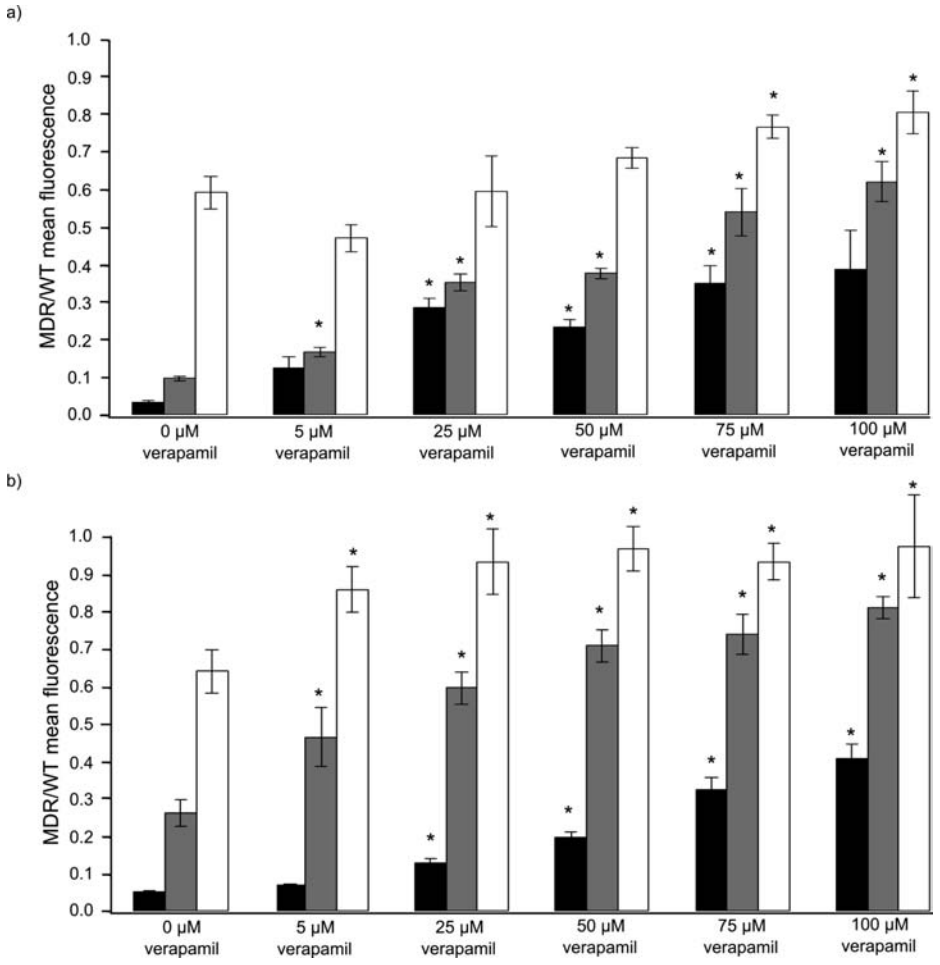

Figure 5. Representative accumulation ratio of MDR to WT cells of (a) rhodamine alone and (b) mPEG-rhodamine conjugates. Black bars represent Rho6G and mPEG-Rho6G, gray bars represent Rho123 and mPEG-Rho123, and white bars represent RhoB and mPEG-RhoB. Conjugates follow the same trends as the dyes alone with increasing verapamil concentrations. Also, the pattern of high (Rho6G), medium (Rho123), and low (RhoB) P-gp efflux of the free dyes is maintained with conjugation of mPEG. All bars are an average of 3 replicates. * represents statistical significance of $p < 0.01$ over 0 μM verapamil condition.

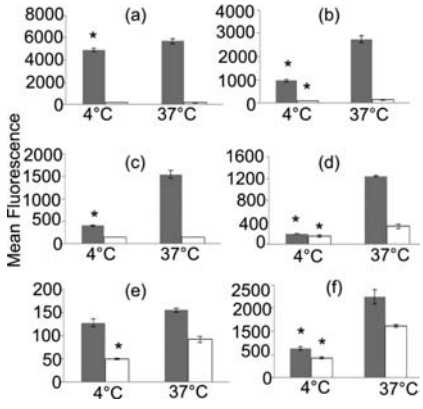

Figure 6. FACS analysis comparing accumulation of (a) Rho6G, (b) mPEG-Rho6G, (c) Rho123, (d) mPEG-Rho123, (e) RhoB, and (f) mPEG-RhoB at 4 °C to accumulation at 37 °C. Gray bars represent accumulation in WT cells and white bars represent accumulation in MDR cells. Conjugates have a greater change in accumulation than native dyes with the temperature change, signifying endocytosis as an internalization mechanism. * represents statistical significance of $p < 0.01$.

reported here.[16,17] Confirmation of P-gp mediated efflux of the mPEG-rhodamine conjugates was accomplished by serial increases in the concentration of verapamil. Verapamil is a well-established inhibitor of P-gp that increases intracellular accumulation of free Rho6G, free Rho123, and free RhoB in a concentration dependent manner. Higher concentrations of verapamil lead to higher accumulation of Rho6G,[35,36] Rho123,[37,38] and RhoB[39] in MDR cell lines. Our results show that higher concentrations of verapamil increase accumulation of all dyes and conjugates in MDR cells. Rho6G has significant increases in MDR/WT accumulation ratio above 25 μM of verapamil. At 100 μM of verapamil there is a large variance in accumulation ratio leading to an insignificant result compared to 0 μM. This is likely due to variability in P-gp expression between cells in the MDR cell line and the strength of Rho6G as a P-gp substrate. The mPEG-Rho6G conjugate has a significant increase in accumulation ratio at all verapamil concentrations and still remains a strong P-gp substrate. Both Rho123 and mPEG-Rho123 have significant increases in MDR/WT accumulation ratio with as little as 5 μM of verapamil and are moderately effluxed by P-gp. RhoB does not show significant increases until 75 μM of verapamil and mPEG-RhoB shows an accumulation ratio close to 1 after 25 μM of verapamil, signaling that both are less effective P-gp substrates.

dx.doi.org/10.1021/bc5002196 | *Bioconjugate Chem.* 2014, 25, 1462−1469

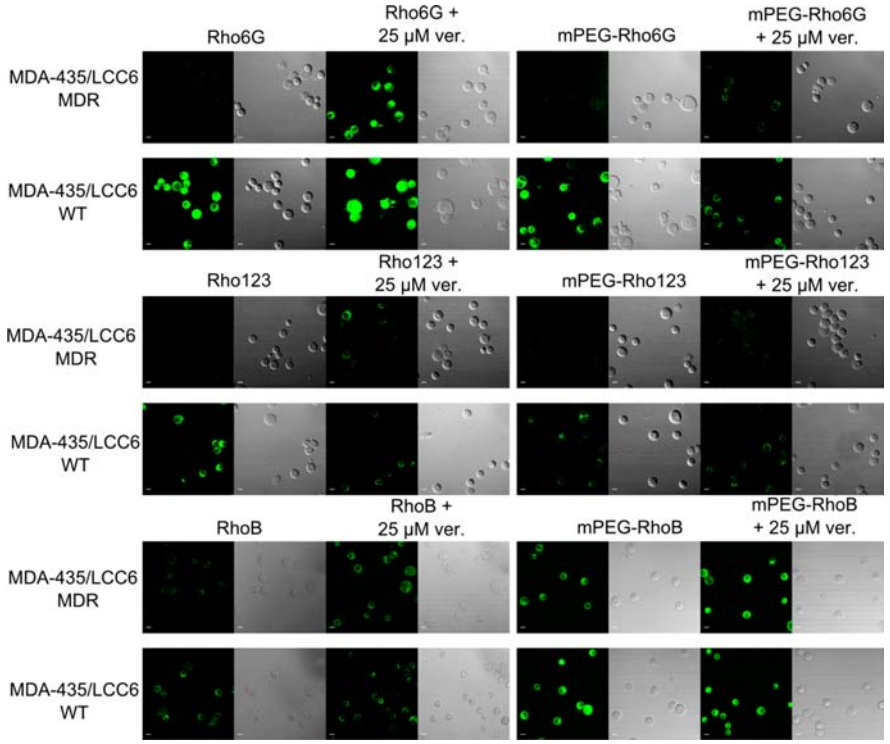

Figure 7. Confocal images of MDR and WT cells incubated with mPEG-Rho123, mPEG-Rho6G, mPEG-RhoB, Rho123, Rho6G, or RhoB. Cells were incubated with 0 μM or 25 μM verapamil, both at 37 °C. Fluorescent accumulation is greater in WT cells for all conditions at 0 μM verapamil. At 25 μM verapamil fluorescent accumulation is similar for both MDR and WT cells for all conditions. Scale bar represents 10 μm.

Polymer conjugates of P-gp substrates have previously been reported for doxorubicin.[40] These conjugates were designed to allow escape from P-gp mediated efflux by covalently attaching polymers at the amine site on doxorubicin, which is essential for P-gp binding.[41] However, for the mPEG-substrates reported in this study, the amine groups on the substrates are preserved allowing for the conjugates to remain P-gp substrates.

FACS analysis was also performed following 4 °C incubation. mPEG-Rho6G, mPEG-Rho123, and mPEG-RhoB all show significant decreases in accumulation in both MDR and WT cells suggesting endocytosis as the mechanism of cell entry, a well-characterized internalization mechanism for macromolecules.[13,42−44] The conjugates are still able to interact with P-gp during endocytosis, as P-gp has been shown to retain activity.[45] Rho6G and Rho123 show significant decreases in accumulation for WT cells, but not for MDR cells due to efficient efflux at 37 °C. The decrease in Rho6G is much less than in mPEG-Rho6G due to the difference in passive diffusion versus endocytosis. Rho123 and mPEG-Rho123 have similar decreases in WT accumulation due to the fact that Rho123 shows little accumulation in non-MDR cell lines.[46] RhoB has a significant decrease in both WT and MDR cell lines, since P-gp mediated efflux for this substrate at 37 °C is poor.

Confocal images were taken to visualize the FACS results at 0 μM and 25 μM verapamil. Fluorescence is visible in all WT cell lines for all conditions. In all cases, when 25 μM verapamil is introduced fluorescence is similar in MDR cells lines as in WT cell lines.

CONCLUSION

Strategies to investigate MDR-expressing cancerous tumors can greatly benefit from macromolecuar P-gp substrates. This study demonstrates that conjugation of Rho6G and Rho123 through the 2′-position to mPEG produces conjugates that can still be classified as P-gp substrates. FACS analysis was used to determine the efflux patterns of mPEG-Rho6G, mPEG-Rho123, and commercially available mPEG-RhoB conjugates in MDA-435/LCC6 MDR and MDA-435/LCC6 WT cells. Confocal imaging provided visual verification of FACS data. The knowledge that Rho conjugates still act as P-gp substrates makes rhodamine dyes a reasonable choice as a tethered system for further analysis of P-gp interactions *in vitro* and *in vivo*.

MATERIALS AND METHODS

Materials. Dialysis tubing of 2000 g/mol molecular weight cutoff (MWCO) was purchased from Spectrum Laboratories (Rancho Dominguez, CA). Deuterated dimethyl sulfoxide was purchased from Cambridge Isotope Laboratories (Andover, MA). Methoxypolyethylene glycol amine (mPEG-NH_2), rhodamine 123 (Rho123), rhodamine 6G (Rho6G), rhodamine B (RhoB), anhydrous dimethylformamide (DMF), triethylamine (TEA), RIPA buffer, phosphate buffered saline (PBS) with calcium and magnesium, protease inhibitor cocktail, monoclonal anti-P-glycoprotein antibody produced in mouse, monoclonal anti-β-actin antibody produced in mouse, anti-mouse antibody produced in goat, and BCIP-blue liquid substrate were purchased from Sigma-Aldrich (Saint Louis, MO). Methoxypolyethylene glycol rhodamine B (mPEG-RhoB) was purchased from Nanocs (New York, NY). PD-10 columns were purchased from GE Healthcare Biosciences (Piscataway, NJ). Accutase, penicillin/streptomycin, NOVEX Bis-Tris 10% gels, and MOPS running buffer were purchased from Life Technologies (Grand Island, NY). PVDF membrane was purchased from Pall Corporation (Port Washington, NY). Nonfat dry milk blotting grade blocker was purchased from Bio-Rad (Hercules, CA). Sterile cell culture phosphate buffered

dx.doi.org/10.1021/bc5002196 | *Bioconjugate Chem.* 2014, 25, 1462−1469

saline (PBS) and fetal bovine serum (FBS) were purchased from Cellgro (Manassas, VA). HyClone MEM Richter's modification with L-glutamine and phenol red was purchased from Thermo Scientific (Rockford, IL). T-flasks were purchased from Corning (Corning, NY). MDA-435/LCC6 WT and MDA-435/LCC6 MDR cells were graciously donated by Dr. Robert Clarke (Georgetown University, Washington, D.C.) and MD Anderson Cancer Center (Houston, TX).

Synthesis of mPEG-Rho6G and mPEG-Rho123. For production of mPEG-Rho6G, the mPEG-NH_2 (M_n 5000, 241.6 mg, 4.8×10^{-5} mol) was dissolved in anhydrous DMF (2 mL) with excess TEA at room temperature. Excess TEA was added to Rho6G powder (77.2 mg, 1.6×10^{-4} mol) which was then dissolved in anhydrous DMF (12 mL) with slight heating. For production of mPEG-Rho123, mPEG-NH_2 (M_n 5000, 71.6 mg, 1.4×10^{-5} mol) was dissolved in anhydrous DMF (1 mL) with excess TEA at room temperature. Excess TEA was added to Rho123 powder (10.8 mg, 2.8×10^{-5} mol) which was then dissolved in anhydrous DMF (1 mL) at room temperature. For both mPEG-Rho6G and mPEG-Rho123 production, the two DMF solutions were combined and stirred at 30 °C for 1 week while being protected from light with an aluminum foil cover. The solution was then diluted with Milli-Q water (38 mL) and dialyzed (MWCO 2000g/mol) in the dark against deionized water with 14 water exchanges over 1 week at room temperature. After dialysis the solution was dried to a light pink powder by lyophilization in the dark for 3 days. Product yields for mPEG-Rho6G and mPEG-Rho123 were 54.7% and 83%, respectively. ^{1}H NMR and diffusion ordered NMR were conducted on an Inova 600 MHz spectrometer at 25 °C. mPEG-Rho6G conjugate: ^{1}H NMR (600 MHz, DMSO-d_6) δ (ppm): 3.24 (s, 3H, C**H**$_3$O mPEG), 3.5 (s, 4H, C**H**$_2$C**H**$_2$O mPEG), 6.06 (s, 2H, ArH Rho6G), 6.26 (s, 2H, ArH Rho6G), 6.97 (d, 1H, ArH Rho6G), 7.50 (m, 2H, Ar**H** Rho6G), 7.77 (d, 1H, Ar**H** Rho6G), 1.86 (s, 6H, ArC**H**$_3$), 1.21 (t, 6H,NCH$_2$C**H**$_3$). mPEG-Rho123 conjugate: ^{1}H NMR (600 MHz, DMSO-d_6) δ (ppm): 3.17 (s, 3H,C**H**$_3$O mPEG), 3.44 (s, 4H, C**H**$_2$C**H**$_2$O mPEG), 6.09 (s, 1H, Ar**H** Rho123), 6.10 (s, 1H, Ar**H** Rho123), 6.14 (d, 1H, Ar**H** Rho123), 6.16 (d, 1H, Ar**H** Rho123), 6.26 (d, 1H, Ar**H** Rho123), 7.43 (m, 4H, Ar**H** Rho123), 7.68 (d, 1H, Ar**H** Rho123). For diffusion ordered NMR of the mPEG-Rho6G conjugate and mPEG-NH_2 with free Rho6G, the gradient pulse was incremented in 12 steps and 16 steps, respectively. For the diffusion ordered NMR of the mPEG-Rho123 conjugate and mPEG-NH_2 with free Rho123, the gradient pulse was incremented in 16 steps and 12 steps, respectively. Stejskals-Tanner plots were made to represent the intensity decrease with increasing gradient. Points were included on the plots until the peaks had disappeared. The proposed structures of the resulting conjugates are shown in Figure 1 along with the structure of purchased mPEG-RhoB.

Purification of mPEG-RhoB. Purchased mPEG-RhoB was further purified by dissolving the purchased powder in Milli-Q water and passing the sample through a series of PD-10 columns. In brief, the column was equilibrated with 25 mL of Milli-Q water. After equilibration, 2.5 mL of a 6 mg/mL mPEG-RhoB solution was passed through the column followed by elution with 3.5 mL of Milli-Q water. Eluent (3.5 mL) was collected and run through a second column that was also equilibrated with 25 mL of Milli-Q water and eluted with 4.5 mL of Milli-Q water. A clear separation of the high and low molecular weight components was observed in the second column and only the high molecular weight fraction was collected and lyophilized to dryness.

Cell Culture. MDA-435/LCC6 MDR and MDA-435/LCC6 WT cells were maintained at 37 °C with 5% CO_2 in Richter's modified MEM (IMEM) containing L-glutamine, phenol red, 10% fetal bovine serum, and 1% penicillin/streptomycin in 25 cm^2 canted T-flasks.

P-Glycoprotein Detection by Western Blot. Total protein was extracted from 4×10^6 of both MDA-435/LCC6 WT and MDA-435/LCC6 MDR cells by incubating in RIPA buffer (0.5 mL) with 1% protease inhibitor cocktail for 1 h on ice. Cell lysate and any remaining debris were separated by centrifugation at 16 000×*g* for 2 min. Protein was quantified using the BCA protein assay. Cellular protein (50 μg) was separated on a 10% Bis-Tris NOVEX gel with MOPS running buffer at a constant current of 80 mA. Proteins were transferred to a PVDF membrane at 300 mA for 45 min and then 350 mA for an additional 45 min. After blocking in nonfat milk, the membrane was incubated with a 1:5000 dilution of primary anti-P-glycoprotein antibody and 1:8000 dilution of primary anti-β-actin antibody for 1 h followed by incubation for 30 min with a 1:3600 dilution of secondary anti-mouse antibody with alkaline phosphatase. The membrane was developed with BCIP blue liquid substrate.

P-Glycoprotein Interactions. MDA-435/LCC6 WT or MDA-435/LCC6 MDR cells (1×10^6 each) were detached from the culture flask surface with Accutase then incubated in suspension (in Accutase) with 27 μM of either mPEG-Rho6G, mPEG-Rho123, or mPEG-RhoB or 0.27 μM of free Rho6G, free Rho123, or free RhoB for 1 h at either 37 or 4 °C. For inhibition studies the cells were first incubated at 37 °C with 0, 5, 25, 50, 75, or 100 μM verapamil for 20 min then incubated with mPEG-Rho6G conjugate, mPEG-Rho123 conjugate, mPEG-RhoB conjugate, free Rho6G, free Rho123, or free RhoB for an additional hour at 37 °C. Inhibition studies evaluated with confocal imaging were conducted with 25 μM of verapamil since this was determined to be the lowest effective concentration from the FACS experiments. All studies were conducted with the cells gently suspended by rotation during the incubation time. After incubation the cells were centrifuged at 300 rcf for 10 min. The supernatant was removed and the cells were washed once with PBS. They were centrifuged again and resuspended in PBS with calcium and magnesium and placed on ice until FACS or confocal imaging analysis. The two centrifugation steps were included to allow time for efflux. FACS analysis was performed on a BD LSR II FACS (San Jose, CA) machine equipped with a 488 nm laser and 100 000 cells were counted for each trial. Each experimental condition was conducted in triplicate. Data for mPEG-Rho6G, mPEG-Rho123, free Rho6G, and free Rho123 were collected under a FITC filter at a voltage of 300 V. Data for mPEG-RhoB and free RhoB were collected under a PE filter at a voltage of 300 V. FACS data were analyzed by gating all cell populations based on untreated cells. Imaging was performed on a Leica (Buffalo Grove, IL) SP2 confocal microscope with a 40× objective at 488 nm wavelength for fluorescent measurements of mPEG-Rho6G, mPEG-Rho123, free Rho6G, and free Rho123. A 543 nm wavelength was used for fluorescent measurements of mPEG-RhoB and free RhoB. For visual clarification images of cells incubated with RhoB and mPEG-Rho123 were adjusted for brightness by an equal amount for all images. Statistical significance was determined by Student's *t* test with a *p*-value of <0.01 for all dyes and conjugates.

■ ASSOCIATED CONTENT

Supporting Information

^{1}H NMR of mPEG-Rho6G and mPEG-Rho123. This material is available free of charge via the Internet at http://pubs.acs.org.

■ AUTHOR INFORMATION

Corresponding Author

*E-mail: dap43@cornell.edu. Address: Department of Biomedical Engineering, 147 Weill Hall, Cornell University, Ithaca, NY 14853.

Notes

The authors declare no competing financial interest.

■ ACKNOWLEDGMENTS

This work was made possible by a Graduate Fellowship to L.C. from the National Science Foundation, NMR expertise from Dr. Ivan Keresztes at the Cornell University NMR facility, Cornell University Biotechnology Resource Center and cell line donation from MD Anderson Cancer Center.

■ REFERENCES

(1) Eckford, P. D. W., and Sharom, F. J. (2009) ABC efflux pump-based resistance to chemotherapy drugs. *Chem. Rev. 109*, 2989−3011.

(2) Szakács, G., Paterson, J. K., Ludwig, J. a, Booth-Genthe, C., and Gottesman, M. M. (2006) Targeting multidrug resistance in cancer. *Nat. Rev. 5*, 219−234.

(3) Borst, P., Evers, R., Kool, M., and Wijnholds, J. (2000) A family of drug transporters: the multidrug resistance-associated proteins. *J. Natl. Cancer Inst. 92*, 1295−1302.

(4) Aller, S. G., Yu, J., Ward, A., Weng, Y., Chittaboina, S., Zhuo, R., Harrell, P. M., Trinh, Y. T., Zhang, Q., Urbatsch, I. L., and Chang, G. (2009) Structure of P-glycoprotein reveals a molecular basis for poly-specific drug binding. *Science 323*, 1718−1722.

(5) Kim, R. B. (2002) Drugs as P-glycoprotein substrates, inhibitors, and inducers. *Drug Metab. Rev. 34*, 47−54.

(6) Matsuo, H., Wakasugi, M., Takanaga, H., Ohtani, H., Naito, M., Tsuruo, T., and Sawada, Y. (2001) Possibility of the reversal of multidrug resistance and the avoidance of side effects by liposomes modified with MRK-16, a monoclonal antibody to P-glycoprotein. *J. Controlled Release 77*, 77−86.

(7) Iwahashi, T., Okochi, E., Ariyoshi, K., Watabe, H., and Aã-na, E. (1993) Specific targeting and killing activities of anti-p-glycoprotein monoclonal antibody MRK16 directed against intrinsically multidrug-resistant human colorectal carcinoma cell lines in the nude mouse model specific targeting and killing activities of anti-P. *Cancer Res. 53*, 5475−5482.

(8) Thomas, H., and Coley, H. M. (2003) Overcoming multidrug resistance in cancer: an update on the clinical strategy of inhibiting p-glycoprotein. *Cancer Control 10*, 159−165.

(9) Pires, M. M., Hrycyna, C. a, and Chmielewski, J. (2006) Bivalent probes of the human multidrug transporter P-glycoprotein. *Biochemistry 45*, 11695−11702.

(10) Pires, M. M., Emmert, D., Hrycyna, C. A., and Chmielewski, J. (2009) Inhibition of P-glycoprotein-mediated paclitaxel resistance by reversibly linked quinine homodimers. *Mol. Pharmacol. 75*, 92−100.

(11) Kang, J. S., Deluca, P. P., and Lee, K. C. (2009) Emerging PEGylated drugs. *Expert Opin. Emerg. Drugs 14*, 363−380.

(12) Greenwald, R. B. (2001) PEG drugs: an overview. *J. Controlled Release 74*, 159−171.

(13) Werle, M. (2008) Natural and synthetic polymers as inhibitors of drug efflux pumps. *Pharm. Res. 25*, 500−511.

(14) Kabanov, A. V., Batrakova, E. V., and Alakhov, V. Y. (2002) Pluronic block copolymers as novel polymer therapeutics for drug and gene delivery. *J. Controlled Release 82*, 189−212.

(15) Batrakova, E. V., Li, S., Vinogradov, S. V., Alakhov, V. Y., Miller, D. W., and Kabanov, a V. (2001) Mechanism of pluronic effect on P-glycoprotein efflux system in blood-brain barrier: contributions of energy depletion and membrane fluidization. *J. Pharmacol. Exp. Ther. 299*, 483−93.

(16) Eytan, G. D., Regev, R., Oren, G., Hurwitz, C. D., and Assaraf, Y. (1997) Efficiency of P-glycoprotein-mediated exclusion of rhodamine dyes from multidrug-resistant cells is determined by their passive transmembrane movement rate. *Eur. J. Biochem. 248*, 104−112.

(17) Loetchutinat, C., Saengkhae, C., Marbeuf-Gueye, C., and Garnier-Suillerot, A. (2003) New insights into the P-glycoprotein-mediated effluxes of rhodamines. *Eur. J. Biochem. 270*, 476−485.

(18) Nare, B., Prichard, R. K., and Georges, E. (1994) Characterization of rhodamine 123 binding to P-glycoprotein in human multidrug-resistant cells. *Mol. Pharmacol. 45*, 1145−1152.

(19) Störmer, E., von Moltke, L. L., Perloff, M. D., and Greenblatt, D. J. (2002) Differential modulation of P-glycoprotein expression and activity by non-nucleoside HIV-1 reverse transcriptase inhibitors in cell culture. *Pharm. Res. 19*, 1038−1045.

(20) Tian, R., Koyabu, N., Takanaga, H., Matsuo, H., Ohtani, H., and Sawada, Y. (2002) Effects of grapefruit juice and orange juice on the intestinal efflux of P-glycoprotein substrates. *Pharm. Res. 19*, 802−809.

(21) Fröhlich, M., Albermann, N., Sauer, A., Walter-Sack, I., Haefeli, W. E., and Weiss, J. (2004) In vitro and ex vivo evidence for modulation of P-glycoprotein activity by progestins. *Biochem. Pharmacol. 68*, 2409−2416.

(22) Lee, J. S., Paull, K., Alvarez, M., Hose, C., Monks, A., Grever, M., Fojo, a T., and Bates, S. E. (1994) Rhodamine efflux patterns predict P-glycoprotein substrates in the National Cancer Institute drug screen. *Mol. Pharmacol. 46*, 627−638.

(23) Dujols, V., Ford, F., and Czarnik, A. W. (1997) A long-wavelength fluorescent chemodosimeter selective for Cu(II) ion in water. *J. Am. Chem. Soc. 119*, 7386−7387.

(24) Knauer, K.-H., and Gleiter, R. (1977) Photochromism of rhodamine derivatives. *Angew. Chem., Int. Ed. Engl. 16*, 113.

(25) Adamczyk, M., and Grote, J. (2000) Efficient synthesis of rhodamine conjugates through the 2′-position. *Bioorg. Med. Chem. Lett. 10*, 1539−1541.

(26) Veronese, F. M., and Pasut, G. (2005) PEGylation, successful approach to drug delivery. *Drug Discovery Today 10*, 1451−1458.

(27) Gombar, V. K., Polli, J. W., Humphreys, J. E., Wring, S. a, and Serabjit-Singh, C. S. (2004) Predicting P-glycoprotein substrates by a quantitative structure-activity relationship model. *J. Pharm. Sci. 93*, 957−968.

(28) Leonessal, F., Green, D., Licht, T., Wright, A., Lippman, J., and Clarke, R. (1996) MDR: ascites models of human breast cancer. *Br. J. Cancer 161*, 154−161.

(29) Riordan, J. R., and Ling, V. (1979) Purification of P-glycoprotein from plasma membrane vesicles of Chinese hamster ovary cell mutants with reduced colchicine permeability. *J. Biol. Chem. 254*, 12701−12705.

(30) Tsuruo, T., Iida, H., Yamashiro, M., Tsukagoshi, S., and Sakurai, Y. (1982) Enhancement of vincristine- and adriamycin-induced cytotoxicity by verapamil in P388 leukemia and its sublines resistant to vincristine and adriamycin. *Biochem. Pharmacol. 31*, 3138−3140.

(31) Kubin, R. F., and Fletcher, A. N. (1982) Fluorescence quantum yields of some rhodamine dyes. *J. Lumin. 27*, 455−462.

(32) Johnson, C., Jr. (1999) Diffusion ordered nuclear magnetic resonance spectroscopy: principles and applications. *Prog. Nucl. Magn. Reson. Spectrosc. 34*, 203−256.

(33) Momot, K. I., and Kuchel, P. W. (2003) Pulsed field gradient nuclear magnetic resonance as a tool for studying drug delivery systems. *Concepts Magn. Reson. 19A*, 51−64.

(34) Kaucher, M. S., Lam, Y.-F., Pieraccini, S., Gottarelli, G., and Davis, J. T. (2004) Using diffusion NMR to characterize guanosine self-association: insights into structure and mechanism. *Chemistry 11*, 164−173.

(35) Matsumoto, Y., Sasaoka, N., Tsuchida, T., Fujiwara, T., Nagao, S., and Ohmoto, T. (1992) Fluorescent dye rhodamine 6G as a molecular probe to study drug resistance of C6 rat glioma cells. *J. Neurooncol. 13*, 217−222.

(36) Mihályi, A., Gáspár, R., Zalán, Z., Lázár, L., Fülöp, F., and de Witte, P. a M. (2004) Synthesis and multidrug resistance reversal activity of 1,2-disubstituted tetrahydroisoquinoline derivatives. *Anticancer Res. 24*, 1631−1636.
(37) Aguero, B., Saxton, R. E., and Castro, D. J. (1994) Verapamil increases rhodamine 123 laser phototherapy of drug-resistant human sarcoma cells. *J. Clin. Laser Med. Surg. 12*, 193−198.
(38) Yumoto, R., Murakami, T., Nakamoto, Y., Hasegawa, R., Nagai, J., and Takano, M. (1999) Transport of rhodamine 123, a P-glycoprotein substrate, across rat intestine and Caco-2 cell monolayers in the presence of cytochrome P-450 3A-related compounds. *J. Pharmacol. Exp. Ther. 289*, 149−155.
(39) Tutundjian, R., Minier, C., Le Foll, F., and Leboulenger, F. (2002) Rhodamine exclusion activity in primary cultured turbot (*Scophthalmus maximus*) hepatocytes. *Mar. Environ. Res. 54*, 443−447.
(40) Minko, T., Kopecková, P., and Kopecek, J. (1999) Comparision of the anticancer effect of free and HPMA copolymer-bound adriamycin in human ovarian carcinoma cells. *Pharm. Res. 16*, 986−996.
(41) Priebe, W., and Perez-Soler, R. (1993) Design and tumor targeting of anthracyclines able to overcome multidrug resistance: a double-advantage approach. *Pharmacol. Ther. 60*, 215−234.
(42) Kopecek, J., Kopecková, P., Minko, T., Lu, Z. R., and Peterson, C. M. (2001) Water soluble polymers in tumor targeted delivery. *J. Controlled Release 74*, 147−58.
(43) Kopecek, J., Kopecková, P., Minko, T., and Lu, Z. (2000) HPMA copolymer-anticancer drug conjugates: design, activity, and mechanism of action. *Eur. J. Pharm. Biopharm. 50*, 61−81.
(44) De Duve, C., De Barsy, T., Poole, B., Trouet, A., Tulkens, P., and Van Hoof, F. (1974) Lysosomotropic agents. *Biochem. Pharmacol. 23*, 2495−2531.
(45) Fu, D., and Arias, I. M. (2012) Intracellular trafficking of P-glycoprotein. *Int. J. Biochem. Cell Biol. 44*, 461−464.
(46) Sarver, J. G., Klis, W. a., Byers, J. P., and Erhardt, P. W. (2002) Microplate screening of the differential effects of test agents on Hoechst 33342, Rhodamine 123, and Rhodamine 6G accumulation in breast cancer cells that overexpress p-glycoprotein. *J. Biomol. Screen. 7*, 29−34.